J. Fluid Mech. (1988), *vol.* 192, *pp.* 393–419
Printed in Great Britain

A numerical study of three-dimensional stratified flow past a sphere

By HIDESHI HANAZAKI

Division of Atmospheric Environment, National Institute for Environmental Studies, Tsukuba, Ibaraki 305, Japan

(Received 22 May 1987)

A numerical study is described of the Boussinesq flow past a sphere of a viscous, incompressible and non-diffusive stratified fluid. The approaching flow has uniform velocity and linear stratification. The Reynolds number Re ($= 2\rho_0 Ua/\mu$) based on the sphere diameter is 200 and the internal Froude number F($= U/Na$) is varied from 0.25 to 200. Here U is the velocity, N the Brunt–Väisälä frequency, a the radius of the sphere, μ the viscosity and ρ_0 the mean density. The numerical results show changes in the flow pattern with Froude number that are in good agreement with earlier theoretical and experimental results. For $F < 1$, the calculations show the flow passing round rather than going over the obstacle, and confirm Sheppard's simple formula for the dividing-streamline height. When the Froude number is further reduced ($F < 0.4$), the flow becomes approximately two-dimensional and qualitative agreement with Drazin's three-dimensional low-Froude-number theory is obtained. The relation between the wavelength of the internal gravity wave and the position of laminar separation on the sphere is also investigated to obtain the suppression and induction of separation by the wave. It is also found that the lee waves are confined in the spanwise direction to a rather narrow strip just behind the obstacle as linear theory predicts. The calculated drag coefficient C_D of the sphere shows an interesting Froude-number dependence, which is quite similar to the results given by experiments. In this study not only C_D but also the pressure distribution which contributes to the change of C_D are obtained and the mechanism of the change is closely examined.

1. Introduction

Stratified flows past an obstacle have been studied both theoretically and experimentally for many years. For two-dimensional flows there are many theoretical results. In some special inviscid cases, the exact governing equations are linear and exact solutions can be obtained (Long 1953, 1955; Yih 1960). But for three-dimensional flows, theoretical results have been obtained only when the disturbance caused by the obstacle is small and the linear approximation is valid (e.g. Crapper 1959, 1962), or when part of the fluid does not go over the top of the obstacle because of the stratification (Sheppard 1956), or when the stratification is very strong and the flow is approximately confined to horizontal planes (Drazin 1961; Brighton 1978).

Sheppard's formula was derived by assuming a fluid parcel, the pressure within which is equal to that of surrounding fluid in hydrostatic balance. Under this assumption and using Bernoulli's theorem, the following integral formula which

would predict the dividing-streamline height z_s was obtained:

$$\tfrac{1}{2}\rho_e U^2(z_s) = g\int_{z_s}^{h}(h-z)\left(-\frac{d\rho}{dz}\right)dz. \tag{1a}$$

Here U is the upstream velocity, ρ_e is the density of the fluid on the dividing streamline, g is the gravitational acceleration and h is the obstacle height. If a fluid parcel is originally at a higher level than z_s, it goes over the top of the obstacle; otherwise it may go around the sides.

This formula is reduced to a simpler form

$$z_s/h = 1-F \quad (F = U/Nh) \tag{1b}$$

under conditions of uniform velocity and linear density gradient. Equations (1a, b) assume that all the kinetic energy is converted into potential energy. When only a portion of the kinetic energy is converted, (1b) becomes

$$z_s/h = 1-\alpha F, \tag{1c}$$

with $\alpha \leqslant 1$ (Hunt & Snyder 1980). α is not necessarily less than 1 because the kinetic energy along a streamline can be increased by the dynamic pressure field set up by the obstacle. But this effect would be small when $F \ll 1$ (Snyder *et al.* 1985).

Baines (1979) obtained $\alpha = 2$ for a barrier with a small gap between one side of the barrier and the sidewall of the tank. But the other side of the barrier was completely attached to the sidewall. Snyder *et al.* (1985) suspect that the large value of α may be due to the 'squashing' phenomenon evident in laboratory experiments on two-dimensional stratified flow. In experiments using a finite-length towing tank, upstream fluid initially existing at heights between the top and bottom of the obstacle must spill over the top of the obstacle when the obstacle comes near the endwall of the tank, because the total mass at those heights has to be conserved. Therefore the initially linear upstream density stratification would break down and the density just upstream of the obstacle becomes nearly constant as is shown in figure 5 of Castro (1987). Baines (1987) disagrees with the opinion of Snyder *et al.* because his experiment was conducted in a sufficiently or 'infinitely' long tank and the observations were made before the reflection of upstream disturbances from the endwall came near the obstacle. Therefore we need some further tests to find the value of α in (1c), though it is not yet clear if the dividing-streamline height is really described by such a simple formula as (1c).

Drazin's low-Froude-number theory assumes as a first approximation ($F \to 0$) that the inviscid flow past a body axisymmetric about a vertical axis is completely horizontal and expressed by the flow around a circular cylinder in each horizontal plane. It then presents the deviation from that state by a series in powers of F^2.

Brighton has extended Drazin's theory to higher orders of F^2, and at the same time has showed explicitly that the vertical displacements Δ of streamlines from their upstream height could be expressed by

$$\Delta(x,y,z) = \frac{2F^2a^2z(x^2-y^2+z^2-a^2)}{(x^2+z^2)^2} \tag{2}$$

in the case of the flow past a sphere with uniform velocity and linear stratification at infinity (see figure 1).

It is clear from (2) that on the upstream stagnation line ($x^2+z^2 = a^2, y = 0$), there

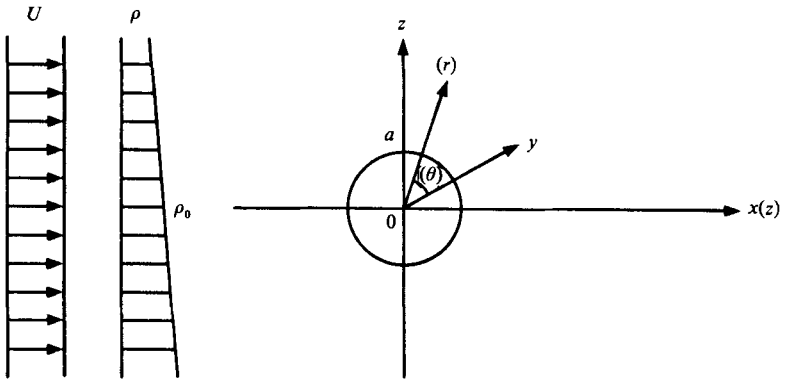

FIGURE 1. Geometry of the flow field, where the cylindrical coordinates are shown in parentheses.

is no displacement, while on the centreplane ($y = 0$, $x^2+z^2 > a^2$), Δ becomes positive or negative in accordance with the sign of z, and on the sphere surface ($x^2+y^2+z^2 = a^2$), Δ takes the opposite sign to z.

Theories by Drazin and Brighton can be applied to finite-amplitude flows, but they break down near the top of the obstacle. Thus experimental or numerical studies are necessary on three-dimensional flows to know the patterns of the entire flow field.

Recently Hunt & Snyder (1980) and Snyder *et al.* (1985) have conducted systematic laboratory experiments which could be compared quantitatively with the existing theories. Hunt & Snyder showed the qualitative validity of Drazin's theory for $F < 0.4$ and Sheppard's formula (1*c*) for $F < 1.0$ (with $\alpha = 1$). They also investigated the flow patterns near the obstacle and discussed the relation between the wavelength of the lee wave and the mechanism of separation by analogy with the two-dimensional flow.

According to linear theory, the wavelength of the lee wave in the flow direction can be approximated by $\lambda = 2\pi U/N = 2\pi F_L L$, where $F_L = U/NL$ and $2L$ is the length of the obstacle, if the channel depth is large enough compared with the obstacle height. When F_L is large and λ is larger than the length of the obstacle $2L$, the wave tends to suppress the eddy region behind the obstacle, but the separation is still controlled by the boundary layer. As F_L decreases and λ becomes almost equal to $2L$, the eddy is completely collapsed. When F_L further decreases and λ becomes shorter than $2L$, the lee wave induces separation on the obstacle.

For the flow past a hemisphere, which may directly correspond to the present study, Snyder, Britter & Hunt (1980) obtained experimental results that confirm the above discussion of low-Froude-number flow and the lee wavelength.

However, only a few results exist for the patterns of the internal wave behind a three-dimensional obstacle. Using triangular ridges, Castro, Snyder & Marsh (1983) investigated the variation of lee-wave amplitude and slope with spanwise aspect ratio. Their results for axial lee wavelength as a function of the Froude number showed good agreement with two-dimensional linear theory even when the aspect ratio was small. Castro (1987) studied the spanwise structure of lee waves for similar ridges and obtained the rate at which the wave amplitude decays across the span. The result compares well with the three-dimensional linear theory by Crapper (1959, 1962), which predicts that lee waves are contained in a strip whose width is comparable with the spanwise length of the obstacle.

The Froude-number dependence of the drag coefficient C_D of a sphere was measured by Lofquist & Purtell (1984) and Mason (1977), and both results show the increase of C_D due to the lee-wave drag as F decreases. But the increased C_D begins to decrease again when F is further reduced. The whole mechanism of these phenomena has not yet been fully understood. Although there are some numerical results for C_D for a two-dimensional obstacle (e.g. Sykes 1978), no quantitative results for three-dimensional flows exist that can be compared directly with laboratory experiments when the obstacle height is not small.

The principal aims of the present work are (i) to closely examine the details of flow patterns and pressure distributions that have never been obtained in laboratory experiments to show how they affect the change of C_D; (ii) to provide a quantitative estimation of the wavelength and the amplitude of the internal gravity wave and discuss the relation between the wavelength and the separation mechanism; and (iii) to test numerically the applicability of the theories by Drazin (1961) and obtain the value of α in Sheppard's formula (1c) at low Froude numbers.

2. Equations of motion and boundary conditions

Let us consider an incompressible and non-diffusive linearly stratified flow past a sphere with uniform upstream velocity (figure 1). The disturbances to uniform flow, including the lee wave and the upstream influence in subcritical range, may be limited to some finite region near the obstacle. This is because waves in three-dimensional flows can diverge laterally and have much lower amplitude compared with two-dimensional waves. In addition linear theory (Su 1975) suggests that the damping effect of viscosity becomes stronger, particularly far from the obstacle. But it is still desirable to get a nearly unbounded flow and reduce the amplitude of the possible upstream columnar motions by locating the upper and lower boundary as far away as possible. Thus in this study the outer boundary is set at about twenty sphere diameters from the sphere in the flow direction and about ten diameters away in the vertical and the spanwise directions (see §3.2).

Under the Boussinesq approximation the dimensional governing equations are written as follows:

$$\frac{\partial \boldsymbol{v}'}{\partial t}+(\boldsymbol{v}'\cdot\boldsymbol{\nabla}')\,\boldsymbol{v}'=-\frac{1}{\rho_0}\boldsymbol{\nabla}p'-\frac{\rho'}{\rho_0}g\hat{\boldsymbol{z}}'+\frac{\mu}{\rho_0}\nabla^2\boldsymbol{v}', \tag{3a}$$

$$\frac{\partial \rho'}{\partial t}+(\boldsymbol{v}'\cdot\boldsymbol{\nabla}')\,\rho'=0, \tag{3b}$$

$$\boldsymbol{\nabla}'\cdot\boldsymbol{v}'=0, \tag{3c}$$

where $\boldsymbol{v}'=(v_x', v_y', v_z')$ is the velocity, p' and ρ' are the perturbation pressure and density respectively, ρ_0 is the mean density, g is the acceleration due to gravity, $\hat{\boldsymbol{z}}'$ is the unit vector along z-axis and μ is the viscosity.

We then non-dimensionalize velocities by the uniform velocity U, distances by the radius of the sphere a, and perturbation pressure by $\rho_0 U^2$ to obtain the equations in dimensionless form:

$$\frac{\partial \boldsymbol{v}}{\partial t}+(\boldsymbol{v}\cdot\boldsymbol{\nabla})\,\boldsymbol{v}=-\boldsymbol{\nabla}p-\frac{1}{F^2}\rho\hat{\boldsymbol{z}}+\frac{2}{Re}\nabla^2\boldsymbol{v}, \tag{4a}$$

$$\frac{\partial \rho}{\partial t}+(\boldsymbol{v}\cdot\boldsymbol{\nabla})\,\rho=0, \tag{4b}$$

$$\boldsymbol{\nabla}\cdot\boldsymbol{v}=0, \tag{4c}$$

where

$$F = \frac{U}{Na}, \quad N^2 = -\frac{g}{\rho_0}\left[\frac{\partial \rho}{\partial z}\right]_{x=-\infty}, \quad Re = \frac{2\rho_0 Ua}{\mu}.$$

The boundary conditions imposed on $\boldsymbol{v}$ and ρ are as follows:

$$\boldsymbol{v} = 0 \quad \text{on the sphere,} \tag{5a}$$

$$\boldsymbol{v} = (1,0,0), \quad \rho = -z \text{ on the upstream boundary,} \tag{5b}$$

$$\frac{\partial \boldsymbol{v}}{\partial x} = \frac{\partial \rho}{\partial x} = 0 \quad \text{on the outer boundary, except upstream.} \tag{5c}$$

In a numerical study of an unbounded stratified flow past a three-dimensional obstacle, neither the squashing phenomenon observed in laboratory experiments nor the permanent upstream disturbances seen in two-dimensional flow can occur (see also the beginning of this section). Then, if the upstream boundary is located sufficiently far from the sphere, we can fix the upstream condition to be uniform and independent of time.

Condition (5*c*) allows the existence of the wave particularly far downstream, though in fact the amplitude of the wave decreases rapidly as x increases as will become clear in §4 (figure 11).

We shall solve (4) subject to (5) for $Re = 200$ over a wide range of $F (0.25 < F < 200)$.

3. Numerical method

3.1. *Numerical procedure*

The numerical method used is essentially the same as that used by Harlow & Welch (1965). In our problem the following diagnostic equation for the pressure is obtained by taking the divergence of (4*a*) and approximating the time derivative with the forward difference:

$$\frac{D^{n+1} - D^n}{\Delta t} + \operatorname{div}\left[(\boldsymbol{v}^n \cdot \nabla)\boldsymbol{v}^n\right] = -\nabla^2 p^n - \frac{1}{F^2}\operatorname{div}(\rho^n \hat{\boldsymbol{z}}) + \frac{2}{Re}\nabla^2 D^n, \tag{6a}$$

where $D = \operatorname{div} \boldsymbol{v}$, and the superscript n denotes the integration time $t = n\Delta t$.

In the above equation D^{n+1} is set equal to zero while D^n is retained to prevent the accumulation of numerical errors and to assure the divergence-free condition $D = 0$ or (4*c*).

Equations (4*a*, *b*) are rewritten in the form

$$\frac{\boldsymbol{v}^{n+1} - \boldsymbol{v}^n}{\Delta t} + (\boldsymbol{v}^n \cdot \nabla)\boldsymbol{v}^n = -\nabla p^n - \frac{1}{F^2}\rho^n \hat{\boldsymbol{z}} + \frac{2}{Re}\nabla^2 \boldsymbol{v}^n, \tag{6b}$$

$$\frac{\rho^{n+1} - \rho^n}{\Delta t} + (\boldsymbol{v}^n \cdot \nabla)\rho^n = 0, \tag{6c}$$

and (6) is solved numerically using finite differences. In a numerical study some boundary conditions for p^n are necessary to solve (6*a*). They are derived from (6*b*) with the first term on the left-hand side being ignored. In fact $\boldsymbol{v}^{n+1} - \boldsymbol{v}^n$ is zero on the sphere surface and on the upstream boundary. On the downstream boundary it is negligibly small and tends to zero as the flow reaches steady state.

The computational procedure is as follows:

(i) Assume appropriate values of $\boldsymbol{v}^n$ and ρ^n at $t = n\Delta t$ and solve (6*a*) by a

successive over-relaxation method to obtain the corresponding pressure p^n. Specifically, as an initial condition, we use uniform velocity and linear stratification, i.e. $\boldsymbol{v}^n = (1, 0, 0)$ and $\rho^n = -z$ except on the sphere surface where $\boldsymbol{v}^n = (0, 0, 0)$ while $\rho^n = -z$.

(ii) Using the known values of p^n, $\boldsymbol{v}^n$ and ρ^n, solve (6*b*, *c*) to obtain $\boldsymbol{v}^{n+1}$ and ρ^{n+1} respectively.

(iii) The process is repeated for the next integration time $t = (n+1)\Delta t$.

(iv) The calculation is continued until almost steady state (typically at about $t = 30$) is attained. Typical CPU time required for each Froude number was 30 hours on a HITACHI M280–H computer at the National Institute for Environmental Studies.

3.2. *Coordinate system and finite-difference scheme*

In this paper cylindrical coordinates are used (figure 1) for the computation, and the grid generation originated by Thames *et al.* (1977) is conducted in (z, r)-plane to transform the plane to the (ξ, η)-plane with equally spaced orthogonal grid lines. Here ξ and η are taken to be integers ($1 \leqslant \xi \leqslant \xi_{\max}$, $1 \leqslant \eta \leqslant \eta_{\max}$) and z and r are described by functions of ξ and η, i.e.

$$z = z(\xi, \eta), \quad r = r(\xi, \eta). \tag{7a, b}$$

To obtain an appropriate form for the transforming function, we first put

$$z^{(0)}(\xi, \eta) = \left(0.5 + 19.5\frac{\eta - 1}{\eta_{\max}}\right)\cos\frac{\xi - 0.5}{\xi_{\max}},$$

$$r^{(0)}(\xi, \eta) = \left(0.5 + 9.5\frac{\eta - 1}{\eta_{\max}}\right)\sin\frac{\xi - 0.5}{\xi_{\max}},$$

where the diameter of the sphere $2a = 1$. Here $\eta = 1$ and $\eta = \eta_{\max}$ correspond to the sphere surface and the outer boundary respectively. Next we move these grid points toward the sphere surface along each ξ-constant line according to

$$d^{(1)}(\xi, \eta) = d^{(0)}(\xi, \eta)\left[1 - \tanh\left(\frac{\eta_{\max} - \eta}{\eta_{\max}}\right)\right]^3$$

with

$$d^{(n)}(\xi, \eta) = \{[z^{(n)}(\xi, \eta) - z^{(0)}(\xi, 1)]^2 + [r^{(n)}(\xi, \eta) - r^{(0)}(\xi, 1)]^2\}^{\frac{1}{2}},$$

($n = 0, 1$), and get $z^{(1)}(\xi, \eta)$ and $r^{(1)}(\xi, \eta)$. Here $d^{(0)}(\xi, \eta)$ is the original distance between each grid point and that on the sphere surface, and $d^{(1)}(\xi, \eta)$ is the distance after the transformation.

A two-dimensional grid so constructed in the (z, r)-plane is rotated about the z-axis to obtain a three-dimensional grid with axisymmetry (figure 2). In the following calculation $35 \times 61 \times 48$ grid points ($\xi_{\max} = 35, \eta_{\max} = 61$) are used in the (ξ, η, θ) directions respectively.

By the grid-generation method described above, we can concentrate grid points near the sphere so that the flow in the laminar boundary layer can be calculated accurately. When $Re = 200$, the depth of the boundary layer around a sphere with no stratification is roughly estimated by $1/Re^{\frac{1}{2}} = 1/200^{\frac{1}{2}} = 7.1 \times 10^{-2}$, while in the above grid $d^{(1)}(1, 12) = 7.0 \times 10^{-2}$. Therefore several mesh points at least exist in the boundary layer even when the boundary layer becomes thinner due to the

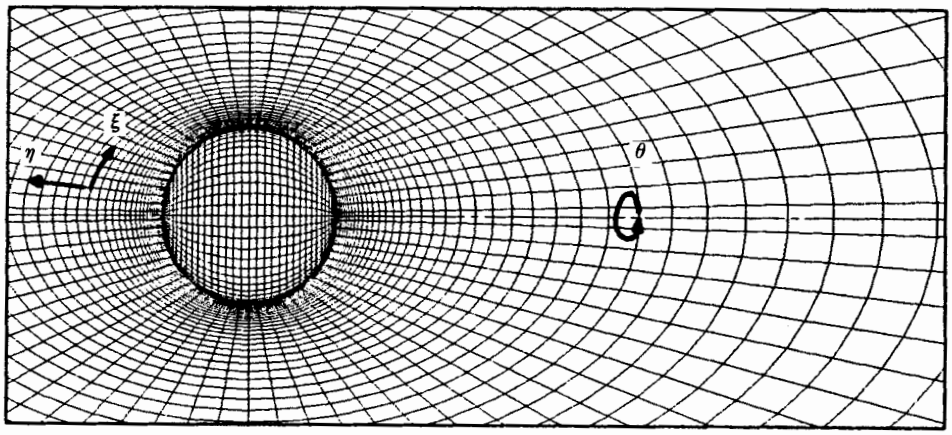

FIGURE 2. Side view of the grid on the centreplane ($y = 0$) and on the sphere surface.

stratification. Though the grid becomes rather coarse far from the sphere, this will have no effect on the solution because the flow is almost uniform there.

When (6) is written in the above cylindrical coordinates, θ being measured from the direction of the y-axis of the Cartesian coordinates, it becomes

$$\nabla^2 p^n = \frac{D^n}{\Delta t} - \operatorname{div}\left[(\boldsymbol{v}^n \cdot \nabla)\,\boldsymbol{v}^n\right] - \frac{1}{F^2}\operatorname{div}(\rho^n \hat{\boldsymbol{z}}) + \frac{2}{Re}\nabla^2 D^n, \tag{8a}$$

$$\frac{u^{n+1}-u^n}{\Delta t} + (\boldsymbol{v}^n \cdot \nabla)\,u^n = -\frac{\partial p^n}{\partial z} + \frac{2}{Re}\nabla^2 u^n, \tag{8b}$$

$$\frac{v^{n+1}-v^n}{\Delta t} + (\boldsymbol{v}^n \cdot \nabla)\,v^n - \frac{v^{2n}}{r} = -\frac{\partial p^n}{\partial r} + \frac{2}{Re}\left(\nabla^2 v^n - \frac{v^n}{r^2} - \frac{2}{r^2}\frac{\partial v^n}{\partial \theta}\right), \tag{8c}$$

$$\frac{w^{n+1}-w^n}{\Delta t} + (\boldsymbol{v}^n \cdot \nabla)\,w^n + \frac{v^n w^n}{r} = -\frac{1}{r}\frac{\partial p^n}{\partial \theta} + \frac{2}{Re}\left(\nabla^2 w^n - \frac{w^n}{r^2} + \frac{2}{r^2}\frac{\partial w^n}{\partial \theta}\right), \tag{8d}$$

$$\frac{\rho^{n+1}-\rho^n}{\Delta t} + (\boldsymbol{v}^n \cdot \nabla)\,\rho^n = 0, \tag{8e}$$

where $\boldsymbol{v} = (v_z, v_r v_\theta) = (u, v, w)$ and the Laplacian

$$\nabla^2 = \frac{\partial^2}{\partial z^2} + \frac{1}{r}\frac{\partial}{\partial r}\left(r\frac{\partial}{\partial r}\right) + \frac{1}{r^2}\frac{\partial^2}{\partial \theta^2}.$$

We then conduct a grid generation and transform derivatives according to

$$\frac{\partial}{\partial z} = \frac{r_\eta \dfrac{\partial}{\partial \xi} - r_\xi \dfrac{\partial}{\partial \eta}}{J}, \quad \frac{\partial}{\partial r} = \frac{z_\xi \dfrac{\partial}{\partial \eta} - z_\eta \dfrac{\partial}{\partial \xi}}{J}, \tag{9a, b}$$

$$\frac{\partial^2}{\partial z^2} = \frac{r_\eta^2 \dfrac{\partial^2}{\partial \xi^2} - 2r_\xi r_\eta \dfrac{\partial^2}{\partial \xi\,\partial \eta} + r_\xi^2 \dfrac{\partial^2}{\partial \eta^2}}{J^2} + \frac{(r_\eta^2 r_{\xi\xi} - 2r_\xi r_\eta r_{\xi\eta} + r_\xi^2 r_{\eta\eta})\left(z_\eta \dfrac{\partial}{\partial_\xi} - z_\xi \dfrac{\partial}{\partial_\eta}\right) + \left(r_\xi^2 z_{\xi\xi} - 2r_\xi r_\eta z_{\xi\eta} + r_\xi^2 z_{\eta\eta}\right)\left(r_\xi \dfrac{\partial}{\partial \eta} - r_\eta \dfrac{\partial}{\partial \xi}\right)}{J^3} \cdots, \tag{9c}$$

where the Jacobian $J = z_\xi r_\eta - z_\eta r_\xi$. Derivatives with respect to θ are unchanged during the grid generation because we use a grid which has a constant $\Delta\theta(= 2\pi/48)$.

Finally we discretize (8) in (ξ, η, θ)-space to conduct the calculation. In that process all space derivatives except convection terms are replaced by the central difference of second order, i.e.

$$\left(\frac{\partial p}{\partial \xi}\right)_{i,j,k} = \frac{p_{i+1,j,k} - p_{i-1,j,k}}{2\Delta\xi} \ldots, \tag{10a}$$

while the convection terms are approximated by a third-order scheme that has been used by Kawamura & Kuwahara (1984) for other problems, i.e.

$$\left(f\frac{\partial u}{\partial \xi}\right)_{i,j,k} = f_{i,j,k}\frac{-u_{i+2,j,k} + 8(u_{i+1,j,k} - u_{i-1,j,k}) + u_{i-2,j,k}}{12\Delta\xi} + |f_{i,j,k}|\frac{u_{i+2,j,k} - 4u_{i+1,j,k} + 6u_{i,j,k} - 4u_{i-1,j,k} + u_{i-2,j,k}}{4\Delta\xi} \ldots, \tag{10b}$$

where f is an arbitrary function and (i,j,k) denotes the grid point in (ξ, η, θ)-space.

The primary error of this scheme is estimated to be

$$(\Delta\xi)^3 |f| \frac{\partial^4 u}{\partial \xi^4}, \tag{10c}$$

which is only slightly dissipative. With this highly accurate scheme, the incompressible condition (6*c*) or (8*e*) can be solved stably even when no diffusion terms are present. When an internal hydraulic jump occurs, artificial viscosity is necessary to reduce the numerical oscillation across the jump. But the use of a scheme with large dissipation often obscures the formation of the jump. The small dissipation effects of (10*b*) will thus also work well in the calculation of the jump.

4. Results

4.1. *The Froude-number dependence of the flow patterns*

When the stratification is very weak ($F = 200$, figures 3*a*, 6*a*), the flow pattern is almost the same as that for no stratification with $Re = 200$ (Taneda 1956; Pruppacher, Le Clair & Hamielec 1970). The axisymmetric standing eddy which separates at about 120° from the upstream stagnation point (figure 5) exists behind the sphere. The pressure distribution on the sphere also shows axisymmetry, and the dynamic pressure in the vertical ($y = 0$) and the horizontal ($z = 0$) planes almost completely coincide (figure 4*a*). At this high Froude number the fluid at all heights far upstream has sufficient kinetic energy to overcome the potential energy required to go over the top of the sphere, so the fluid originally at $z = 0$ covers most of the sphere surface except the eddy region, as is shown by the density distribution given in figure 3(*a* iii). When the flow is steady, it is clear from equations (3*b*) or (4*b*) that the velocity vectors are tangential to the isopycnic surface, so we can assume the isopycnic line in the centreplane to be something like a streamline in that plane because the steady flow is symmetric about $y = 0$ and the y-component of velocity is zero on $y = 0$. Closed streamlines are not seen near the centre of the eddies in figure 3(*a* iii) because the density variation with position is small there. In fact, closed lines also exist in addition to the plotted lines. These closed regions are isolated from the

other fluid three-dimensionally. In non-diffusive flow the density of these regions is determined by the process of the formation of the standing eddy, i.e. by the initial condition. Therefore if the initial condition is abnormal, the result will become unstable. The initial condition used in this study is normal, at least in that the density distribution is the same as for the laboratory experiments. The internal wave is not yet apparent in the figure because the wavelength is still very long.

As the Froude number decreases, the standing eddy collapses mainly vertically and the separation line moves backward (figure 5), because the wavelength of the internal wave becomes shorter and comparable with the diameter of the sphere, to suppress the vertical extent of the eddy. At Froude number 2.0, the effects of the reduced wavelength begin to appear, and the position of the minimum pressure in the vertical plane moves downstream (figure 4*b*) following the delay of separation (figure 5). However, the density distribution still shows that almost all the fluid particles go over the top (figure 3*b*).

At about $F = 1.0$ (figures 3*c*, 4*c*, 6*b*) the standing eddy completely collapses (figure 5) and only wave motions remain downstream of the sphere. It should be noted that the lee wave has nearly its maximum amplitude at this Froude number.

At Froude number 0.7 (figures 3*d*, 4*d*), separation appears again near the leeward stagnation point (figure 5). Under the first crest of the lee wave, the intervals of isopycnic surfaces and the directions of the velocity vectors suddenly change and an internal hydraulic jump occurs. (Because the hydraulic jump in a continuously stratified fluid has not been properly analysed or understood, as Yih (1980) states in his book, we define it in this paper by the criterion described above.) At the same time symmetric horizontal vortices appear downstream near the horizontal plane $z = 0$. Separation in the vertical direction is induced by the internal wave whose length is comparable with the diameter of the sphere $2a$, while the horizontal vortices may be the products of the two-dimensionality of the flow due to strong stratification. The structure of the lee wave and the hydraulic jump can be seen in the side view of velocity vectors in figure 7. Comparing this figure with figure 3(*d*), it is found that the amplitude of the waves decreases very rapidly as y increases, and the waves are mainly confined to a narrow strip just behind the sphere, of width $2a$ in accordance with linear theory (Crapper 1959) and experimental results (Castro 1987). It is also seen that the existence of the hydraulic jump is localized to $|y| < 0.3a$. The tendency of fluid to go round the sides of the sphere becomes evident at this Froude number, and a substantial proportion of the isopycnic lines do not go over the top. Further, it is seen that isopycnic lines with $H_s/a = \pm 0.1$ begin to deflect slightly before they impact on the sphere surface. These deflections balance the vertical pressure gradients caused by the two-dimensionality of the flow, as predicted by Drazin's (1961) theory.

At Froude number 0.5 (figures 3*e*, 4*e*), the separation line moves upstream (figure 5) as the horizontal eddies grow larger. The upstream deflections of isopycnic lines become strong and the downflow near the windward sphere surface also becomes apparent in the side view of velocity vectors. The vorticity distribution (figure 6*c*) also shows the existence of a region with vorticity of opposite sign near the upstream stagnation point.

In figure 3(*d*–*f*), the calculated hydraulic jump is not so strong as that in the experiments by Hunt & Snyder (1980), perhaps because of the difference in the shape of the obstacle and the much lower Reynolds number in this study.

From side views of the flows (figure 3*d*, *e*), it is seen that the phase of the wave varies with height and the wave at the level of the top of the sphere has an advanced

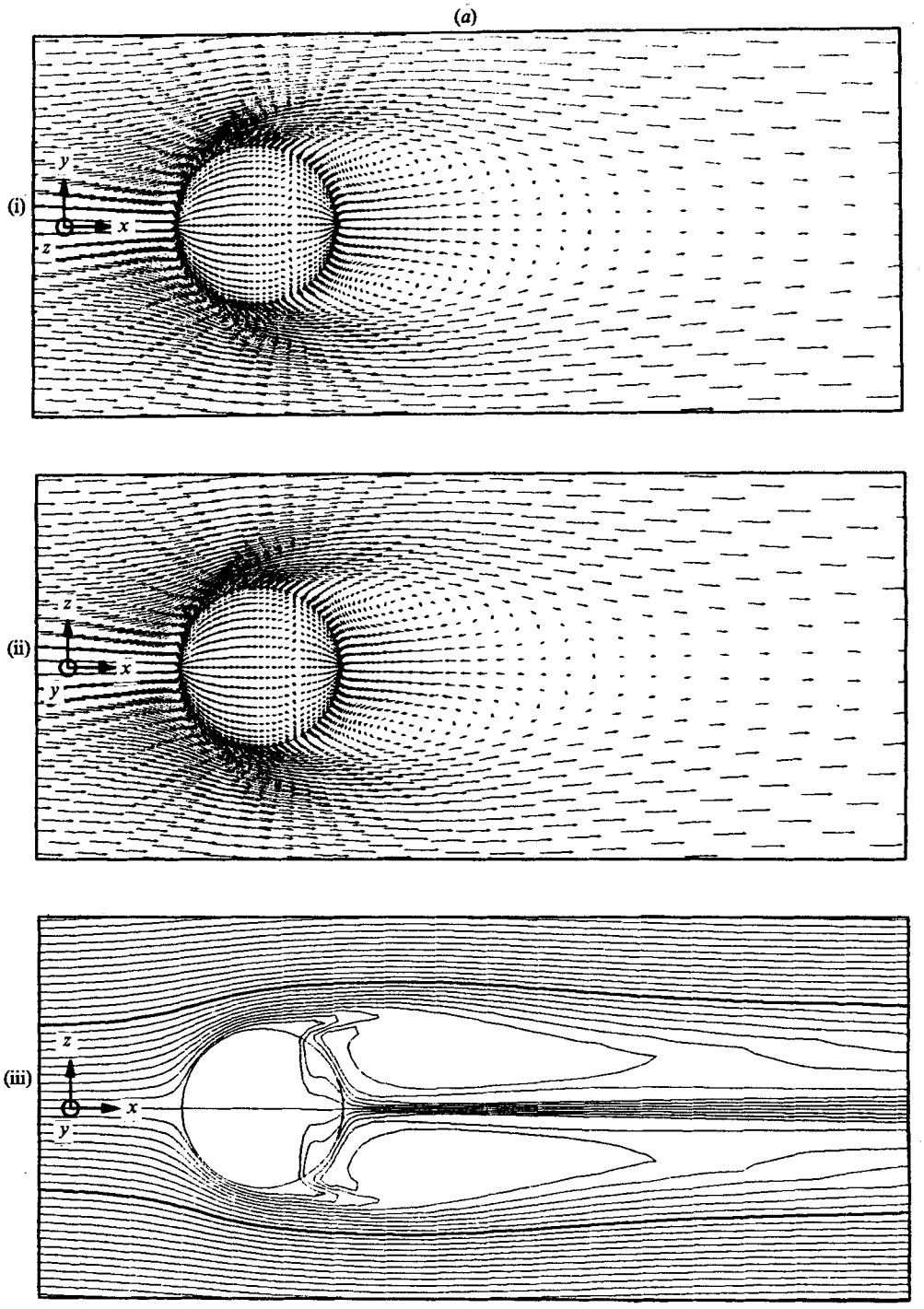

FIGURE 3(*a*). For caption see p. 407.

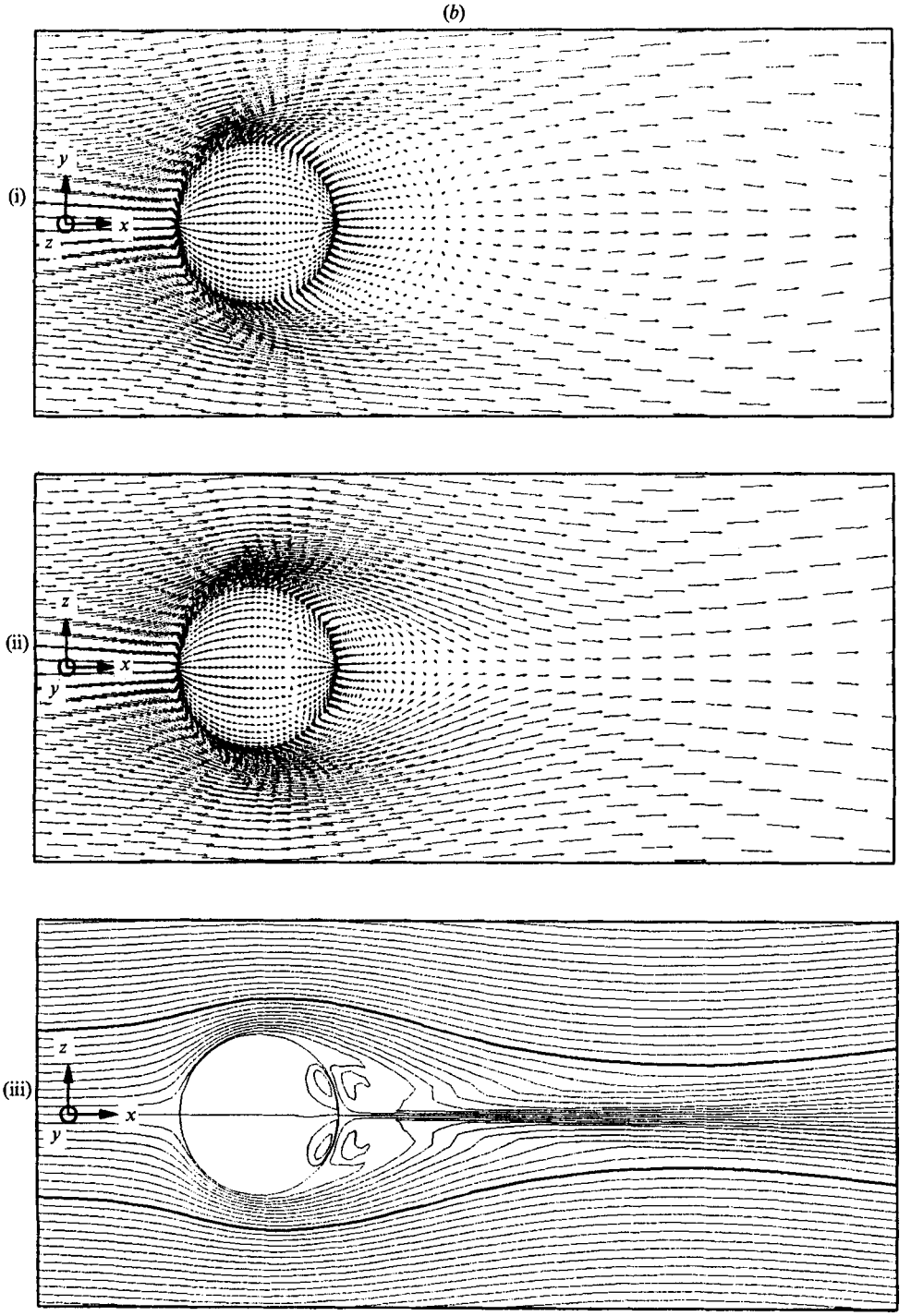

FIGURE 3(*b*). For caption see p. 407.

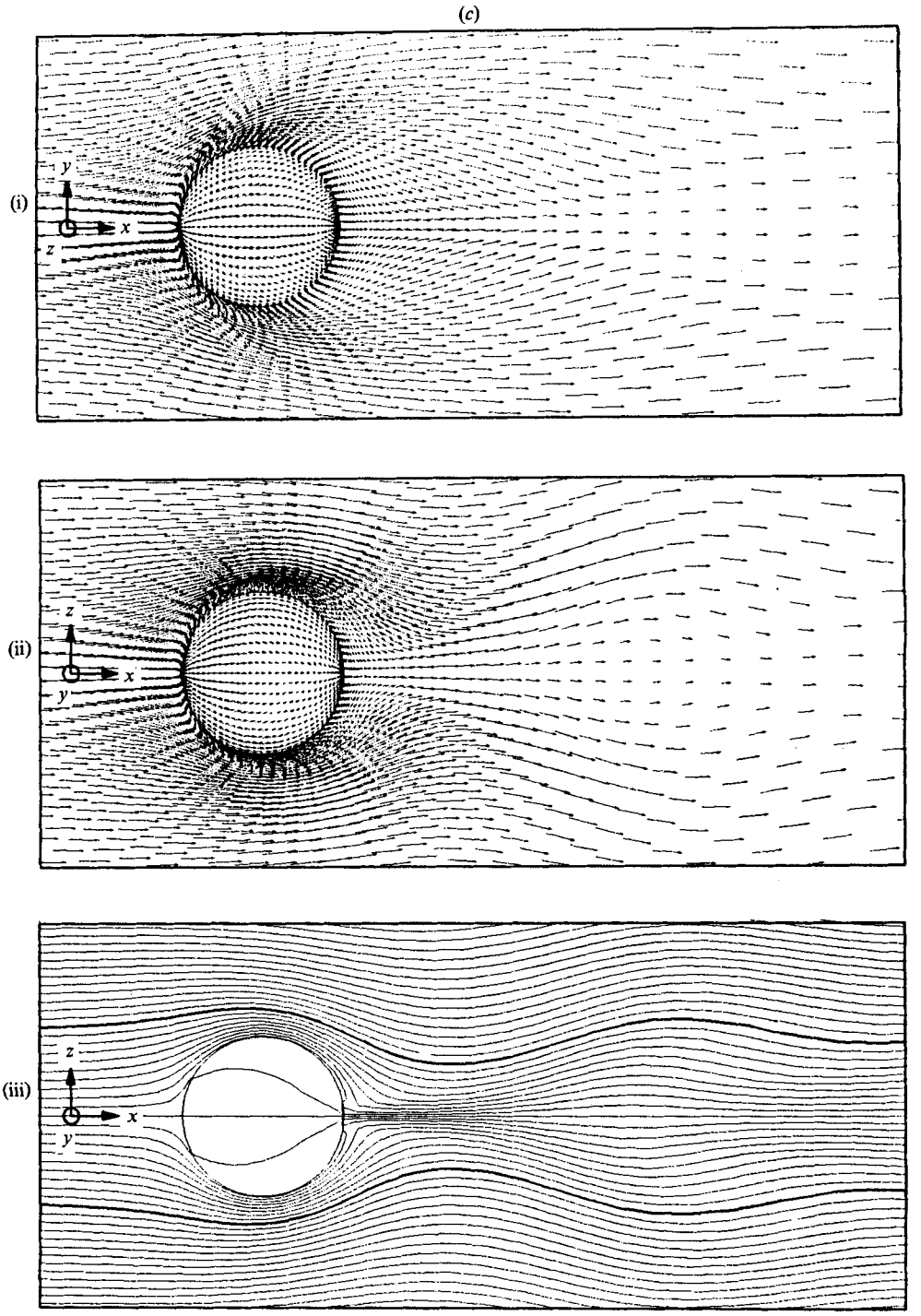

FIGURE 3(*c*). For caption see p. 407.

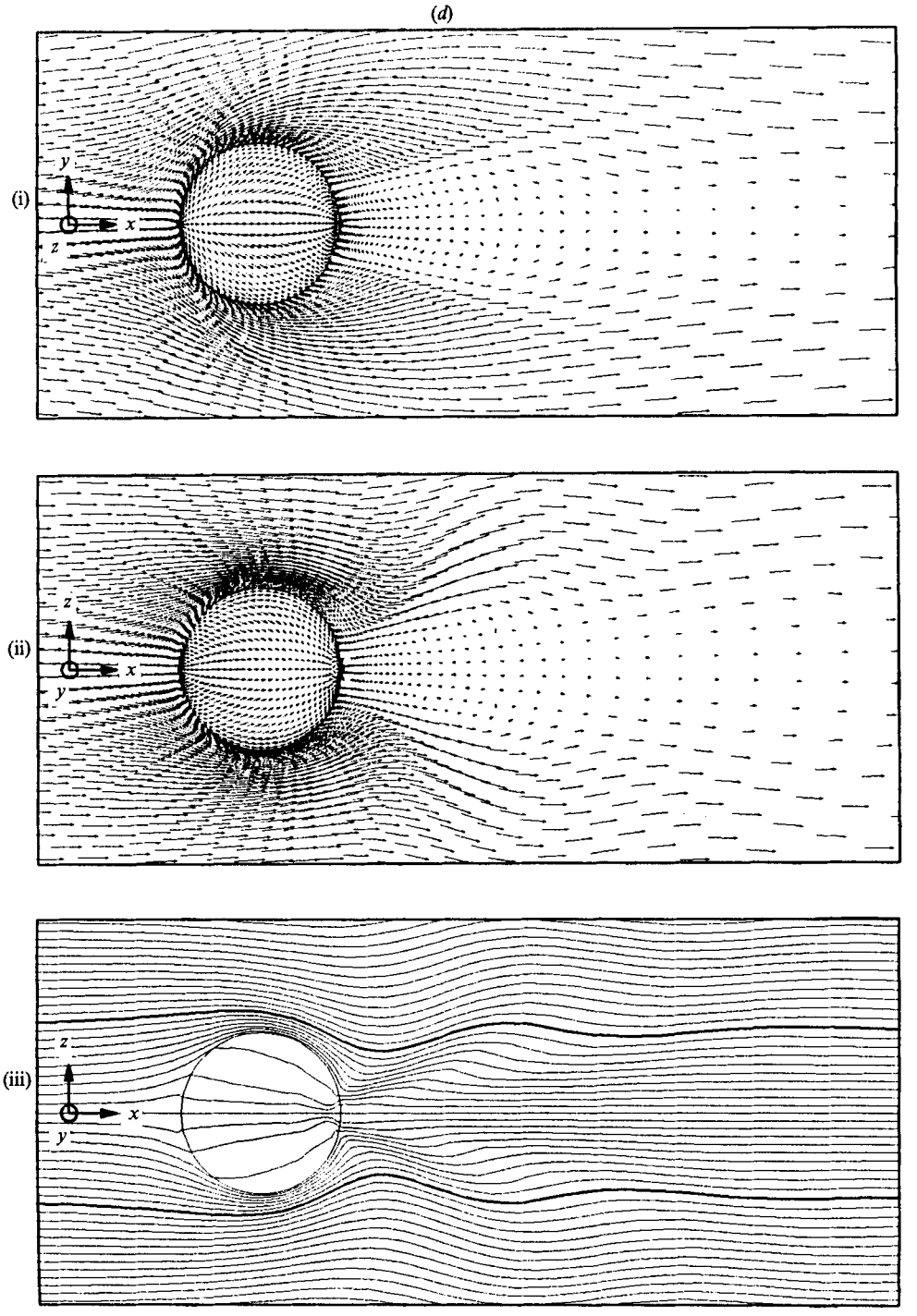

FIGURE 3(*d*). For caption see p. 407.

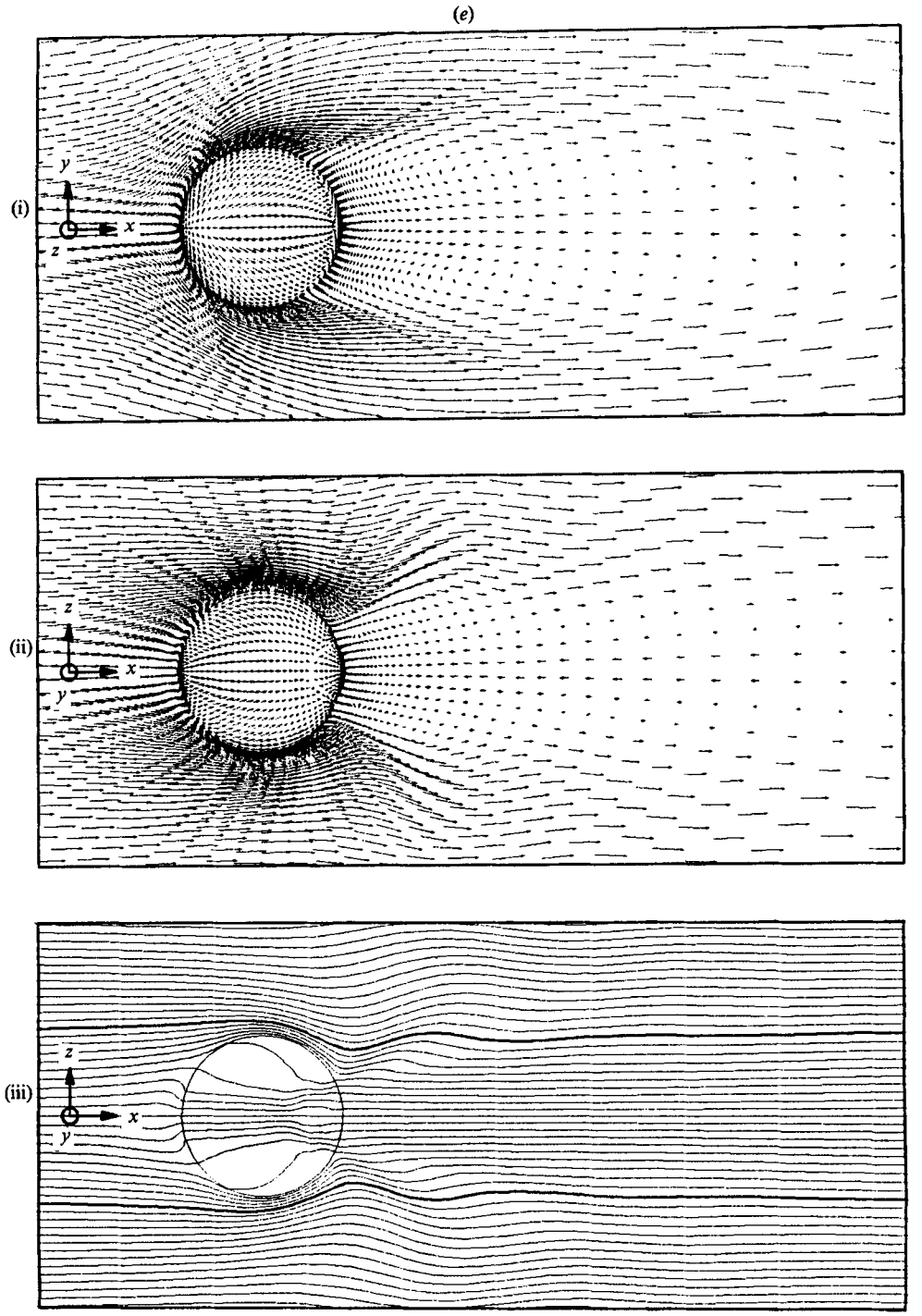

FIGURE 3(*e*). For caption see facing page.

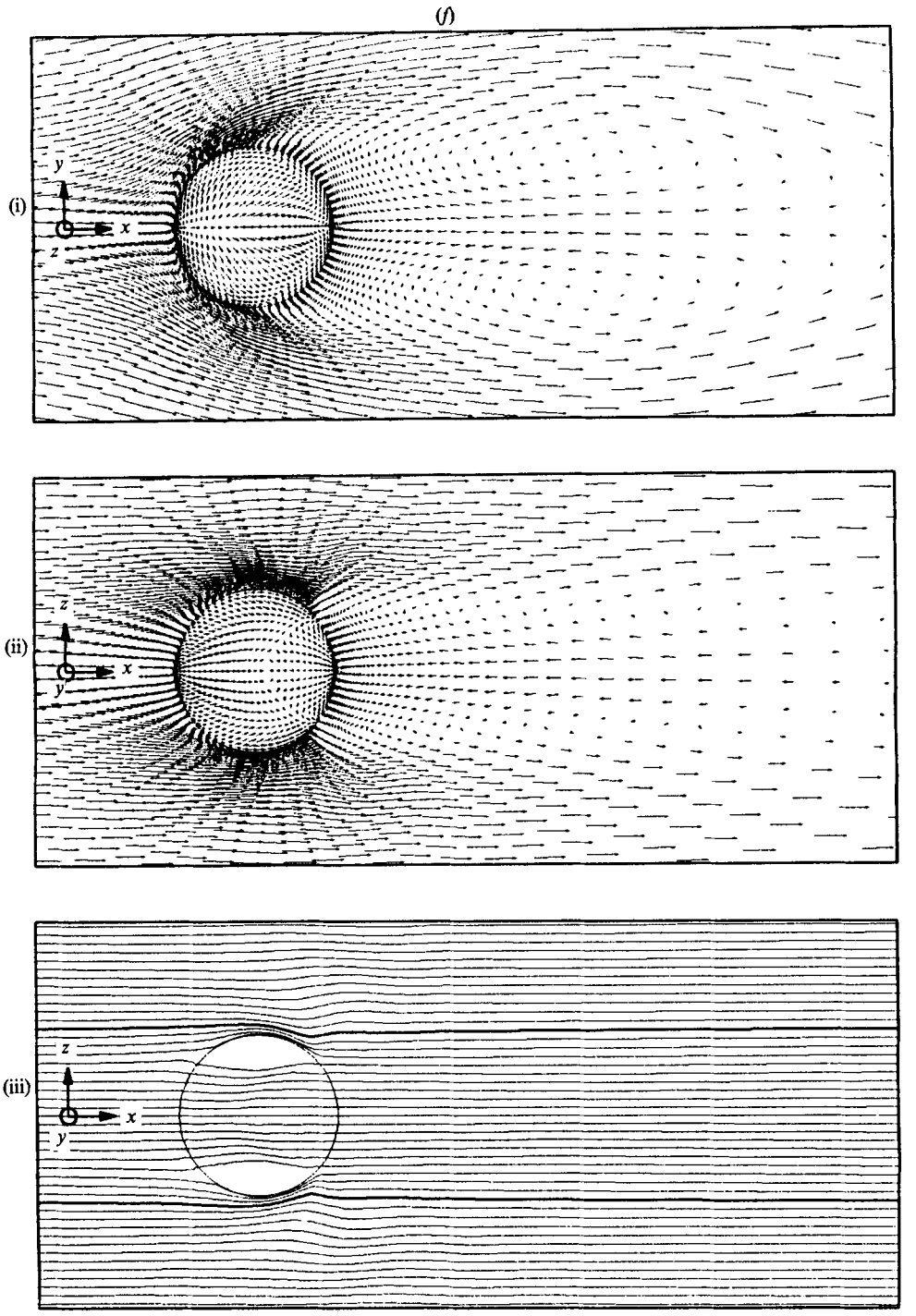

FIGURE 3. Top view of velocity vectors in the horizontal plane ($z = 0$) and on the sphere surface (i), side view of velocity vectors (ii) and isopycnic surfaces (iii) in the centreplane ($y = 0$) and on the sphere surface. Since the velocity on the sphere is zero, the velocity vectors at one mesh point outside the sphere are presented 'on' the sphere surface with their lengths five times enlarged. Isopycnic lines are drawn for $H_s/a = 0, \pm 0.1, \pm 0.2, \ldots$, and broad lines show $H_s/a = \pm 1$. Here H_s is the upstream height of the isopycnic line. (*a*) $F = 200$; (*b*) 2; (*c*) 1; (*d*) 0.7; (*e*) 0.5; (*f*) 0.25.

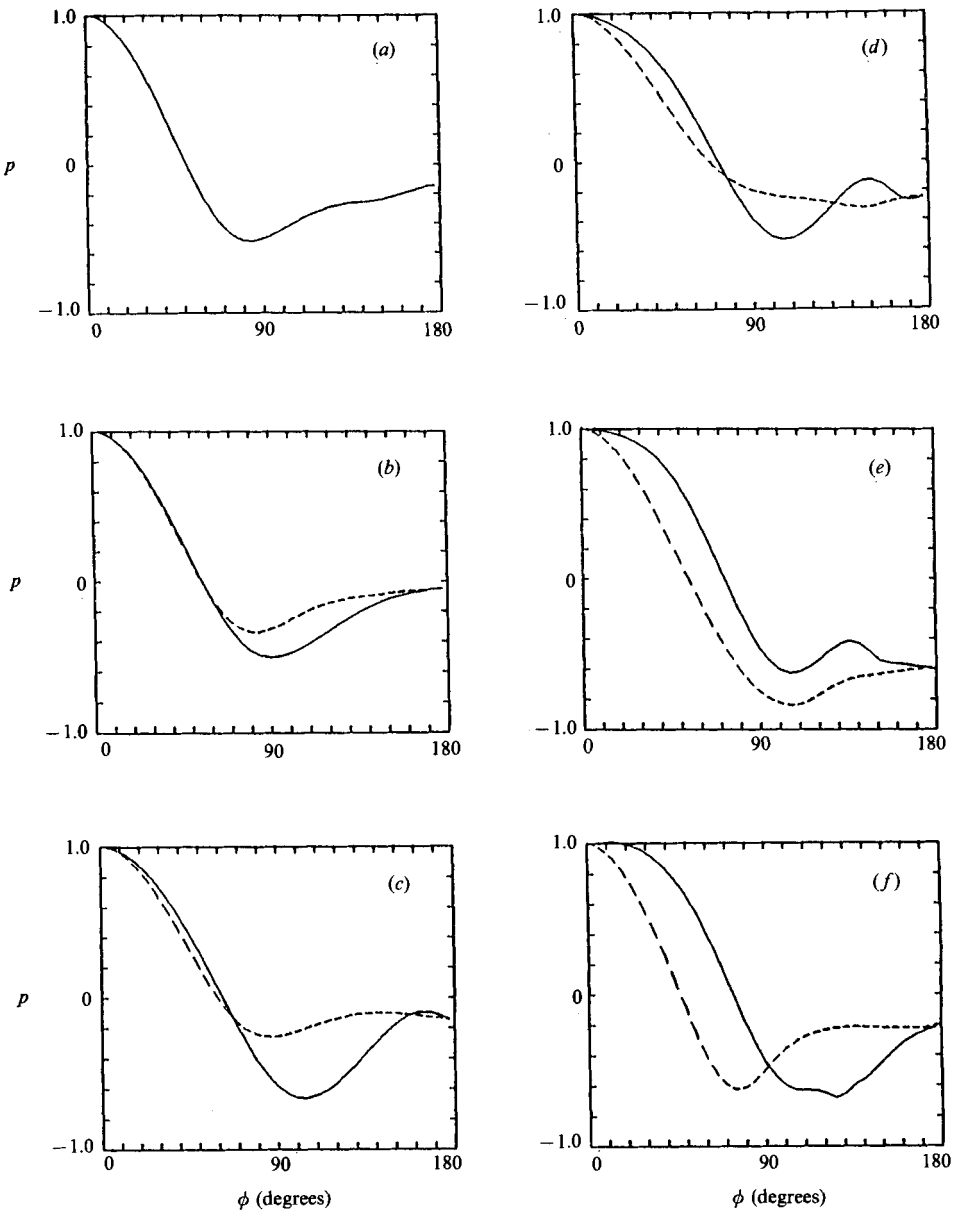

FIGURE 4. Distribution of dynamic pressure on the sphere surface in the vertical ($y = 0$) and horizontal ($z = 0$) planes: ——, vertical; – – –, horizontal. ϕ is measured from the upstream stagnation point. Here the dynamic pressure is obtained by subtracting pressure due to hydrostatic balances from the total pressure. We can discuss the change of C_D using the dynamic pressure on the sphere surface because the hydrostatic pressure works symmetrically on the sphere surface and does not contribute to C_D. (*a*) $F = 200$; (*b*) 2; (*c*) 1; (*d*) 0.7; (*e*) 0.5; (*f*) 0.25.

phase compared with lower waves. This fact may have some relevance for the phase variation with height in vortex shedding at higher Reynolds numbers that was observed by Brighton (1978).

At the lowest Froude number $F = 0.25$ (figures 3*f*, 4*f*), the flow is approximately horizontal except near the top of the sphere, where the fluid has still sufficient energy

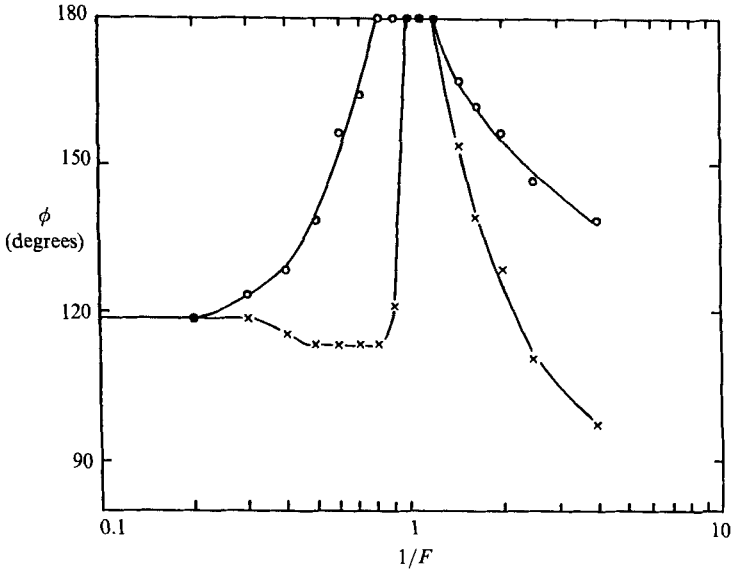

FIGURE 5. Movement of separation points on the sphere with the Froude number in the vertical ($y = 0$) and the horizontal ($z = 0$) planes: —○—, vertical; —×—, horizontal. The angle ϕ of separation is measured from the upstream stagnation point.

to go over the top. Separation in the horizontal plane $z = 0$ occurs at about 90° from the upstream stagnation point, which is approximately the same angle as in the case of the flow around a two-dimensional circular cylinder at $Re = 200$. This fact further confirms the two-dimensionality of the flow near $z = 0$ at this low Froude number. But we must keep in mind that the pressure on the sphere surface facing the horizontal eddy becomes larger with decreasing Froude number, and the resultant value is quite different from that of a circular cylinder. This is presumably due to the vertical interaction of the flow and this is the reason for the drag reduction near this Froude number (figure 8).

4.2. *The Froude-number dependence of the drag coefficient*

From figure 8 we can see that the dependence of ΔC_D on $1/F$ shows fairly good agreement with the previous experiments by Lofquist & Purtell (1984) and Mason (1977). Here ΔC_D is defined by

$$\Delta C_D = C_D(Re, 1/F) - C_D(Re, 0),$$

where

$$C_D(Re, 1/F) = D(Re, 1/F)/(\tfrac{1}{2}\rho_0 U^2 \pi a^2)$$

and D denotes the net drag force on the sphere. Experimental results are not for a constant Reynolds number, while the numerical result is for $Re = 200$. We should mention here that experiments for neutral flow show that $C_D(200, 0) = 0.80$ (Schlichting 1968), and a reliable value of $C_D(200, 0) = 0.81$ was obtained numerically by a non-stratified version of the program used in this study.

In the range of $0 < 1/F < 0.5$, an only slightly negative value of $\Delta C_D = -0.02$, which may be within the range of numerical errors, is observed. But the results by Lofquist & Purtell show a clear reduction in C_D. This may be due to the difference in the Reynolds number. In this study ($Re = 200$), the wake is not turbulent so that vertical suppression of turbulence, which was observed by Lofquist & Purtell for

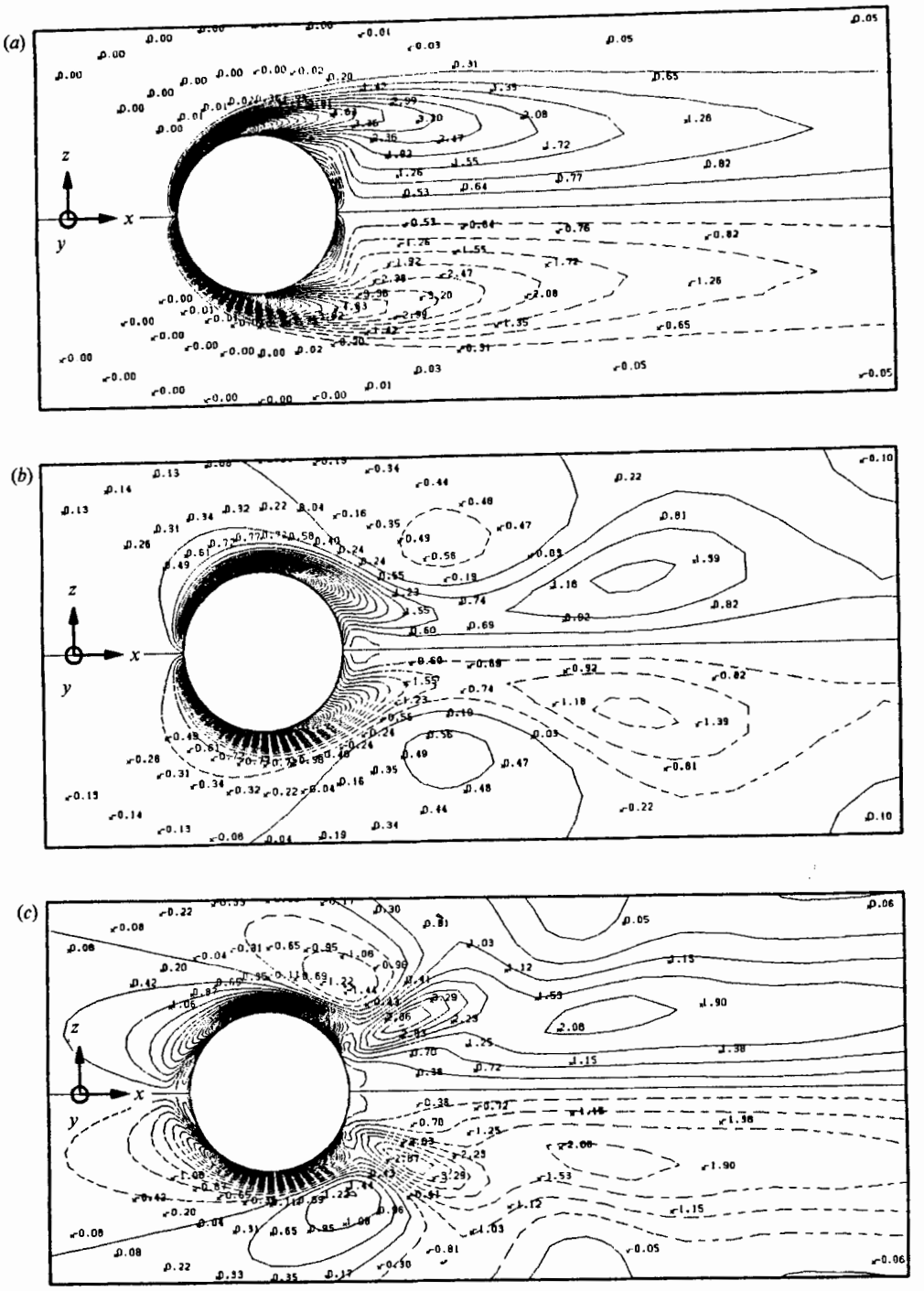

FIGURE 6. Distribution of the y component of vorticity in the centre-plane ($y = 0$). Solid lines show positive values, while dashed lines show negative values. (*a*) $F = 200$; (*b*) 1; (*c*) 0.5.

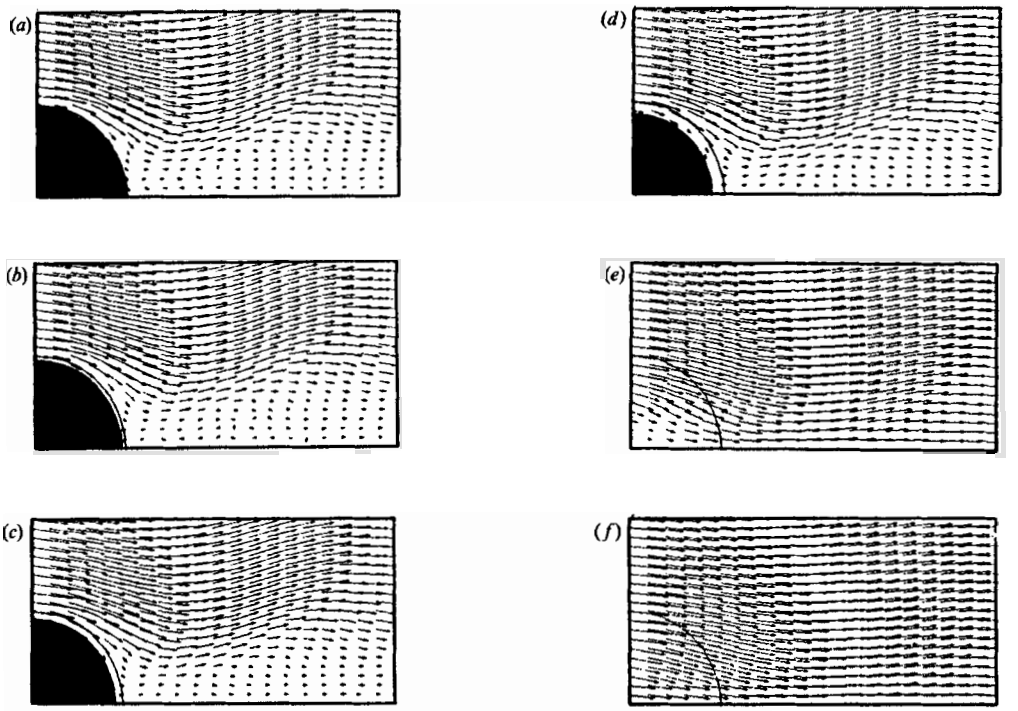

FIGURE 7. Side views of velocity vectors in different vertical planes for $F = 0.7$. To show the variation of wave patterns with the y-coordinate, the originally calculated velocities are interpolated and velocities on orthogonal grid points are presented. (*a*) $y = 0.2a$; (*b*) $0.3a$; (*c*) $0.4a$; (*d*) $0.5a$; (*e*) $1.0a$; (*f*) $1.2a$.

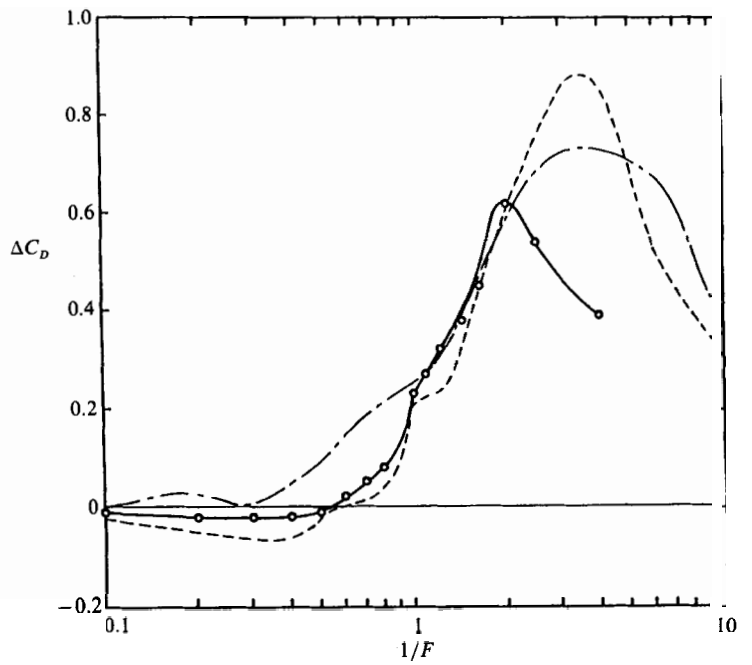

FIGURE 8. Change of ΔC_D as a function of $1/F$: —○—, numerical results; – – –, experiments by Lofquist & Purtell (1984); – · – · –, experiments by Mason (1977).

$Re > 1000$, cannot occur downstream. At first sight it may seem that C_D reduces considerably due to the collapse of the standing eddy. But the lee waves begin to have large amplitude in this range of $1/F$ as seen in figure 11, and these two opposite effects, which tend to increase or decrease the pressure behind the sphere, cancel each other.

In the range of $0.5 < 1/F < 1.0$, ΔC_D increases considerably. In this range (figure 4*b*, *c*), the pressure increases on the windward sphere surface while it decreases on the leeward surface. On the windward side of the sphere, the vertical motions of fluid particles are suppressed by stratification. Thus the fluid is forced to approach the sphere surface at angles closer to 90° to increase the pressure. On the lee side, the amplitude of the lee waves becomes larger as seen in figure 11 and more and more energy is taken up by the waves. So the effect of the lee wave in reducing the pressure overcomes the effect of eddy collapse.

Near $F = 1$ the slope of the curve changes significantly and becomes small. According to the discussion by Lofquist & Purtell, ΔC_D due to the lee wave is estimated by $F^2 \Delta C_D \sim \overline{\delta_m^2}/a$, where δ_m is the vertical amplitude of the Brunt-Väisälä oscillation and the bar denotes its average. In this study $\overline{\delta_m^2}$, i.e. $F^2 \Delta C_D$, reaches its maximum near $1/F = 1$ (figure 11) and this may be the reason of the change in the slope of the graph. But below $F = 1$ the hydraulic jump and the downstream horizontal eddies also appear. Therefore the three phenomena described above together affect the change in ΔC_D for $1/F > 1.0$.

For $1.0 < 1/F < 2.0$, ΔC_D still increases though the amplitude of the wave decreases. In this range an internal hydraulic jump that may consume large energy occurs and this causes the pressure deficit in the lee side (figure 4*d*, *e*) while the effect of the weak horizontal eddy is still small.

In the range of $2.0 < 1/F$, ΔC_D decreases owing to the rather high pressure on the leeward sphere surface facing the strong horizontal eddies (figure 4*f*) as already mentioned in §4.1. In this range the amplitude of the lee waves tends to zero and the hydraulic jump also becomes weak. Therefore these two effects may also contribute to the increase of pressure on the leeward side. On the windward side, the pressure near the ground level $z = 0$ (shown by the dashed line) decreases because the flow is almost two-dimensional and the pressure distribution (for $0° < \phi < 90°$) becomes similar to that around a circular cylinder. The difference in ΔC_D between this study and earlier experiments comes from the Reynolds-number difference. When Re is 200, as in this study, the separation line on the sphere in neutral flow is located at about 120° from the upstream stagnation point, and if the flow becomes almost two-dimensional, separation occurs at about 90° near $z = 0$. So the separation line moves upstream. But when Re is above 500, as in most of earlier experiments, the movement occurs only slightly or not at all. Therefore the effect of the rather high pressure on the rear surface (figure 4*f*) becomes stronger in this study compared with the previous experiments.

Figure 9 shows the increment of pressure drag ΔC_p and frictional drag ΔC_f as function of $1/F$. Here ΔC_p and ΔC_f are defined by

$$\Delta C_p = C_p(Re, 1/F) - C_p(Re, 0), \quad \Delta C_f = C_f(Re, 1/F) - C_f(Re, 0)$$

(with $Re = 200$) respectively. In this study C_p and C_f ($C_D = C_p + C_f$) are calculated using the formulae

$$C_p = \frac{1}{\frac{1}{2}\rho_0 U^2 \pi a^2} \int_S (-p\delta_{ik}) n_k \mathrm{d}S,$$

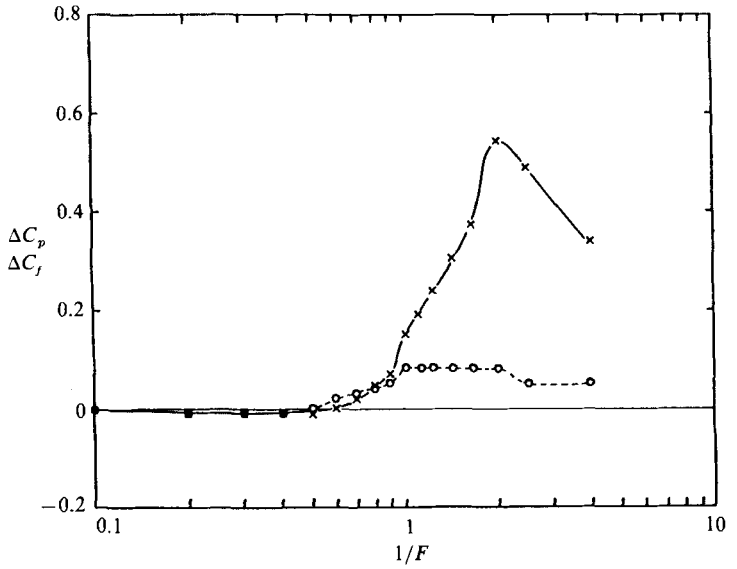

FIGURE 9. Change of ΔC_p and ΔC_f as functions of $1/F$: —×—, ΔC_p; --○--, ΔC_f.

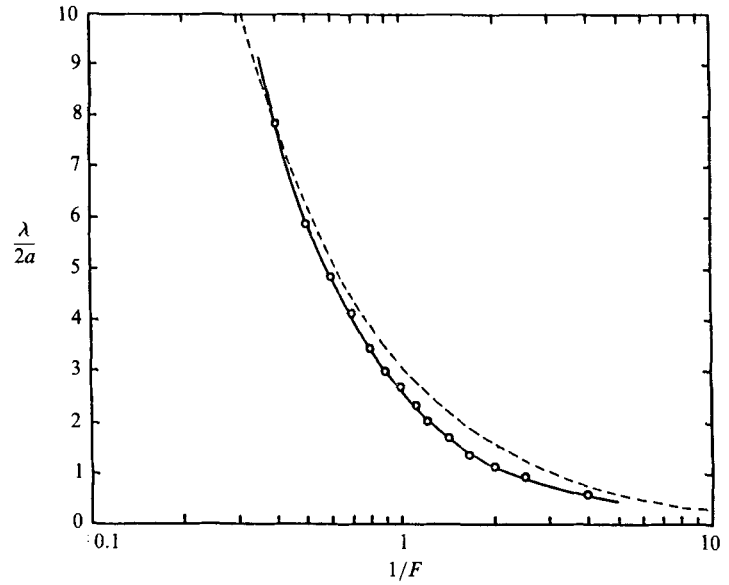

FIGURE 10. Wavelength of internal gravity wave as a function of $1/F$: —○—, numerical results; ----, linear theory. Numerical results are represented by the distance in the x-direction between the first two crests of the wave along the isopycnic line of $H_s/a = 1$ in the centreplane ($y = 0$).

and
$$C_f = \frac{1}{\frac{1}{2}\rho_0 U^2 \pi a^2} \int_S \mu \left(\frac{\partial v_i}{\partial x_k} + \frac{\partial v_k}{\partial x_i} \right) n_k \, \mathrm{d}S,$$

where i is the flow direction, n_k is the unit vector normal to the sphere surface, and the surface integral is calculated on the sphere surface. The density variation with position is ignored in these formulae because we are under the Boussinesq approximation and all the particles on the sphere surface have nearly the same

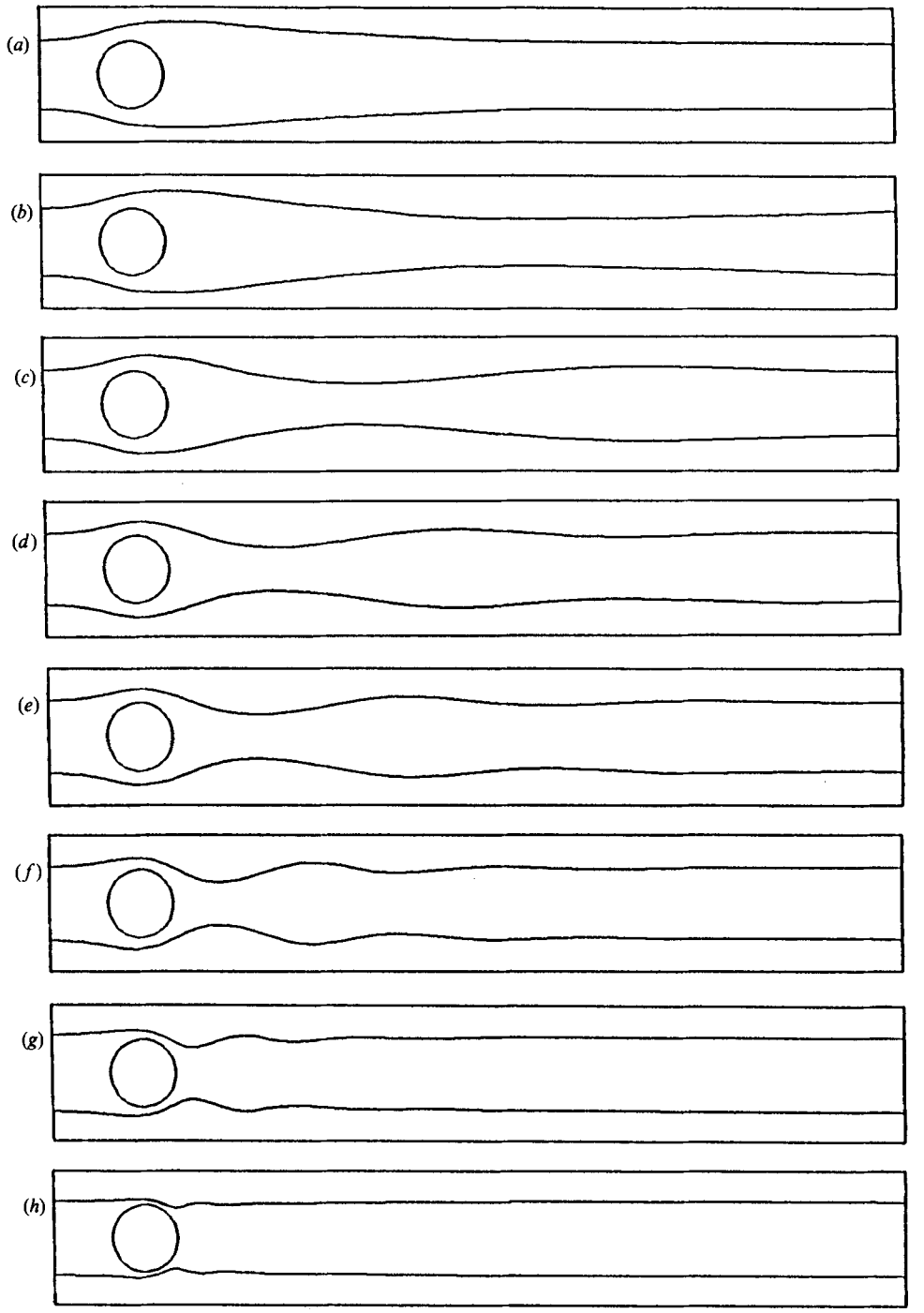

FIGURE 11. Variation of patterns of the internal wave with the Froude number. Isopycnic lines $H_s/a = \pm 1$ in the centreplane ($y = 0$) are depicted. (*a*) $F = 10$; (*b*) 5; (*c*) 2.5; (*d*) 1.67; (*e*) 1.43; (*f*) 1; (*g*) 0.7; (*h*) 0.4.

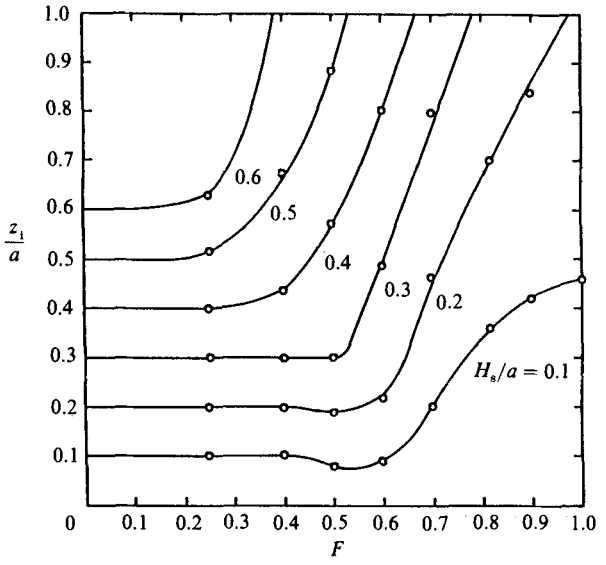

FIGURE 12. Impingement height z_i of isopycnic lines in the centreplane ($y = 0$) as a function of the Froude number.

Froude number	H_s/a at the top of the sphere	α
0.25	0.70	1.20
0.4	0.59	1.03
0.5	0.52	0.96
0.6	0.44	0.93
0.7	0.35	0.93
0.8	0.28	0.90
0.9	0.23	0.86
1.0	0.18	0.82

TABLE 1. Froude-number dependence of α in Sheppard's formula: $z_s/a = 1 - \alpha F$.

density as that on $z = 0$. In laboratory experiments (e.g. Lofquist & Purtell 1984) the density difference between the top and bottom of the sphere is, at most, $\Delta\rho = \rho_0 \times 7.6 \times 10^{-3}$. Therefore we can neglect the effect of density variation with position when we compare the calculated C_D with experimental results.

When figure 9 is compared with figure 8, it is clear that most of ΔC_D comes from ΔC_p and not from ΔC_f. This suggests the possibility of predicting the increase of C_D or the lee wave drag using only inviscid theories.

4.3. *The relation between the wavelength of the lee wave and the mechanism of separation*

In figure 10 it is seen that the wavelength λ of the internal gravity wave coincides, at least qualitatively, with linear theory. Examples of the calculated wave patterns are shown in figure 11 and comparison with figure 5 will clarify how the wavelength on the centreplane ($y = 0$) is concerned with the separation mechanism; i.e. when $F > 1$ and $\lambda/2a \gtrsim 2.5$, decreasing F and λ tends to suppress the eddy behind the

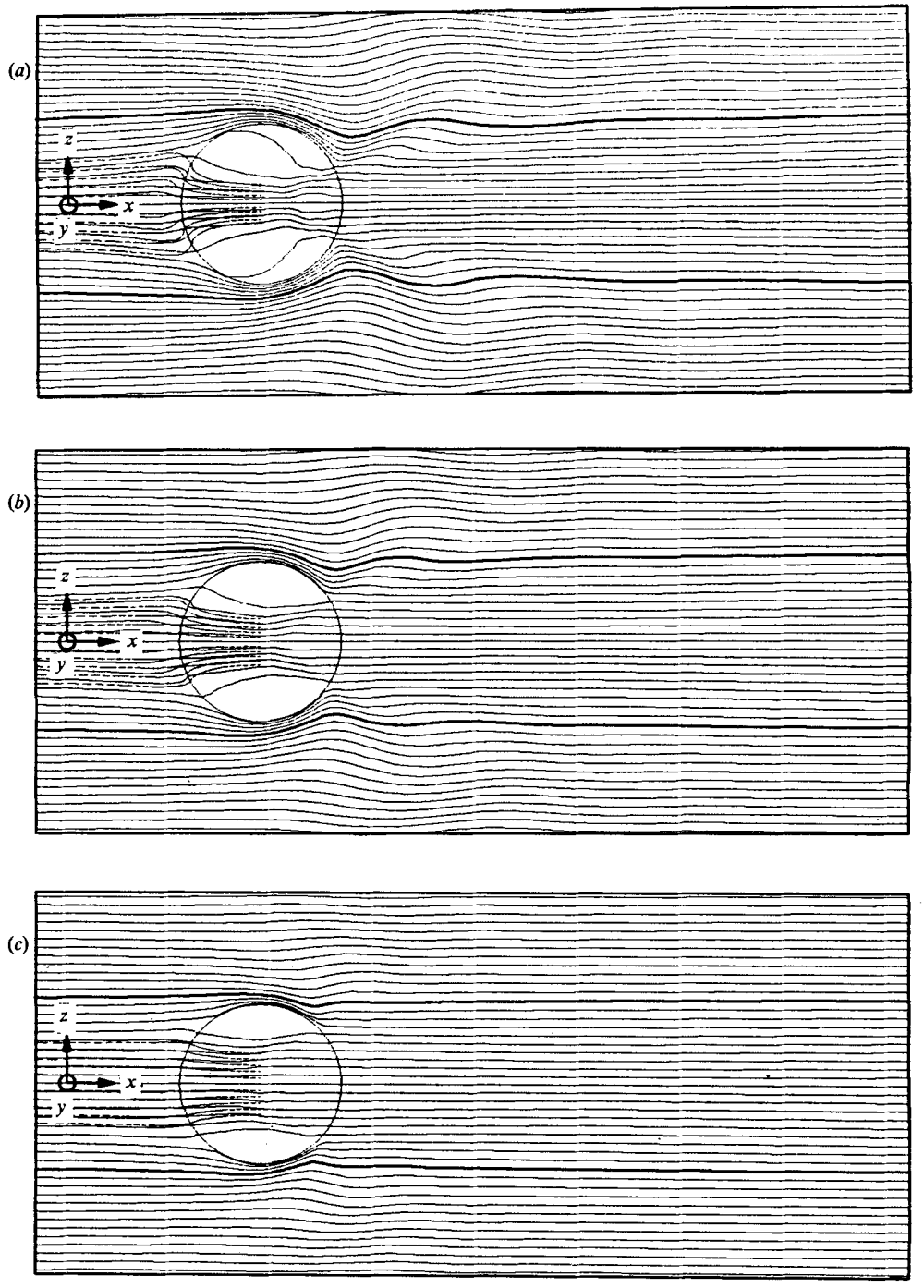

FIGURE 13. Comparison of the numerical results of the isopycnic lines in the centreplane ($y = 0$) and on the sphere surface with Drazin's (1961) theory at low Froude numbers ($F \leqslant 0.5$): ——, numerical results; – – –, theory by Drazin. (*a*) $F = 0.5$; (*b*) 0.4; (*c*) 0.25.

sphere, but when $F < 1$ and $\lambda/2a \lesssim 2.5$, further decrease of F or λ would induce separation on the sphere. The criterion $\lambda/2a = 2.5$ is several times larger than the ideal case described in the introduction (with $L = a$). The difference may come from the very steep slope of the sphere surface near $z = 0$, where the linear approximation breaks down. It also appears that the effective length of the obstacle becomes longer than its real length when the obstacle height is comparable with its length. For example, in the experiments by Hunt & Snyder (1980), the model hill used had a height comparable with its length and the standing eddy completely collapsed at $F = 0.9$ though the lee wavelength was in quite good agreement with linear theory. Anyway, the results show the validity of the extension of the two-dimensional consideration to three-dimensional flow near the centreplane ($y = 0$).

4.4. *Comparison with low-Froude-number theories*

From figure 12 we can see that in the limit of $F = 0$, the flow becomes completely horizontal and impingement height z_i is equal to H_s. As F increases, the value of H_s at the top of the sphere ($= z_s$) decreases.

From table 1 we can see that Sheppard's formula represented by (1*c*) is approximately valid with $\alpha = 1$, but as F increases from 0.25 to 1.0, α decreases from 1.2 to 0.82. The difference between the theory and numerical results near $F = 1$ comes from the fact that even when $F > 1$, part of the fluid does not go over the top of the sphere but goes around the sides because of the stratification. As was already mentioned in the introduction there is a controversy over the value of α in (1*c*). The numerical results are best for $\alpha = 1$ to $\alpha = 2$. In this study the sidewalls are very far from the obstacle and we can consider the result as the flow past a completely isolated three-dimensional obstacle. The situation is, at least approximately, considered to be the same in the experiment of Snyder *et al.* (1985). The experiment by Baines (1979) was conducted for the case with a sidewall very close to the obstacle. Then the fluid is forced to go straight along the sidewall when it has to go around the side of the obstacle. As shown in figure 3(*f*, i), the y-component of velocity in the $z = 0$ plane is large even for $y > 2a$. Therefore his result may be affected by the existence of the sidewall and not represent an isolated obstacle.

Finally, from figure 13, we can see that Drazin or Brighton's theory expressed by (2) is at least qualitatively valid for $F < 0.4$, i.e. as the fluid approaches the sphere it first deflects away from the plane $z = 0$ and then comes back to its original height when it impinges on the sphere surface, and further deflects toward $z = 0$ as it goes around the sides. But the deflection on the side of the sphere is weaker in the numerical results because of the effect of horizontal eddies just downstream.

5. Conclusions

Systematic numerical studies agree with the previous theoretical and experimental results on stratified flows over a three-dimensional obstacle. Though the Reynolds number in this study ($Re = 200$) was low compared with the previous experiments, the resulting flow showed very similar dependence on the Froude number. Of course the location of the separation line on the sphere surface varies with the Reynolds number, which affects the pressure distribution that determines the drag coefficient C_D. But outside the boundary layer and the wake region, the overall pattern of the flow is controlled by the lee waves, which depend only on the Froude number near the obstacle. Therefore the Reynolds number does not have so large an effect as to completely obscure the effects of stratification.

The main results of this study can be summarized as follows.

(i) The increment of the drag coefficient ΔC_D mainly comes from the increment of the pressure drag ΔC_p and not from that of frictional drag ΔC_f. This helps confirm the explanation in the literature for the increase of drag using the inviscid theory of lee waves.

The reduction of the drag coefficient for $F < 0.5$ from its maximum value is due to high pressure on the rear surface of the sphere in the horizontal eddy region. If the two-dimensional flow near $z = 0$ is identical with that of a circular cylinder, the rearward pressure must become much lower. So the 'two'-dimensional flow must have a rather strong vertical interaction.

To study the detailed effect of Re on ΔC_D, it is desirable to make calculations for other higher-Reynolds-number flows ($Re > 200$); and to avoid the influence of Re completely, it is necessary to calculate for $Re > 1000$, where $C_D(Re, 0)$ is nearly independent of Re. But the computation of turbulent flow is outside the scope of the present study.

(ii) The lee waves suppress separation when the Froude number F becomes small, but further reduction of F induces separation, as is shown by earlier experiments.

The region where the lee waves exist is confined in the spanwise (y) direction to a rather narrow strip just behind the sphere, of width roughly the same as the diameter of the sphere, as linear theory predicts. Further, when a hydraulic jump occurs, the wave breaking is only seen near the centreplane ($y = 0$) and the region where it exists is very localized.

(iii) At low Froude numbers Sheppard's formula and Drazin's theory are at least qualitatively valid for $F < 1$ and $F < 0.4$ respectively. The parameter α in Sheppard's formula (1*c*) is not always constant and can vary with the Froude number, but the value is approximately 1 when the obstacle is isolated from other bodies. Drazin's theory is valid for small F, but when the downstream horizontal eddy becomes larger, it affects the flow at the side of the obstacle, and the theory cannot be applied there.

The author would like to thank Dr H. Ueda for giving me this interesting problem, and also Professor H. Takami and Dr T. Miyazaki for their helpful discussions.

REFERENCES

BAINES, P. G. 1979 Observations of stratified flow past three-dimensional barriers. *J. Geophys. Res.* **84**, 7834–7838.

BAINES, P. G. 1987 Upstream blocking and airflow over mountains. *Ann. Rev. Fluid Mech.* **19**, 75–97.

BRIGHTON, P. W. M. 1978 Strongly stratified flow past three-dimensional obstacles. *Q. J. R. Met. Soc.* **104**, 289–307.

CASTRO, I. P. 1987 A note on lee wave structures in stratified flow over three-dimensional obstacles. *Tellus* **39A**, 72–81.

CASTRO, I. P., SNYDER, W. H. & MARSH, G. L. 1983 Stratified flow over three-dimensional ridges. *J. Fluid Mech.* **135**, 261–282.

CRAPPER, G. D. 1959 A three-dimensional solution for waves in the lee of mountains. *J. Fluid Mech.* **6**, 51–76.

CRAPPER, G. D. 1962 Waves in the lee of a mountain with elliptical contours. *Phil. Trans. R. Soc. Lond.* A**254**, 601–623.

DRAZIN, P. G. 1961 On the steady flow of a fluid of variable density over an obstacle. *Tellus* **8**, 239–251.

HARLOW, F. H. & WELCH, J. E. 1965 Numerical calculation of time-dependent viscous incompressible flow of fluid with free surface. *Phys. Fluids* **8**, 2182–2189.

HUNT, J. C. R. & SNYDER, W. H. 1980 Experiments on stably and neutrally stratified flow over a model three-dimensional hill. *J. Fluid Mech.* **96**, 671–704.

KAWAMURA, T. & KUWAHARA, K. 1984 Computation of high Reynolds number flow around a circular cylinder with surface roughness. *AIAA paper* 84-0340.

LOFQUIST, K. E. B. & PURTELL, L. P. 1984 Drag on a sphere moving horizontally through a stratified liquid. *J. Fluid Mech.* **148**, 271–284.

LONG, R. R. 1953 Some aspects of the flow of stratified fluids, I. A theoretical investigation. *Tellus* **5**, 42–58.

LONG, R. R. 1955 Some aspects of the flow of stratified fluids, II. Continuous density gradients. *Tellus* **7**, 342–357.

MASON, P. J. 1977 Forces on spheres moving horizontally in a rotating stratified fluid. *Geophys. Astrophys. Fluid Dyn.* **8**, 137–154.

PRUPPACHER, H. R., LE CLAIR, B. P. & HAMIELEC, A. E. 1970 Some relations between drag and flow pattern of viscous flow past a sphere and a cylinder at low and intermediate Reynolds numbers. *J. Fluid Mech.* **44**, 781–790.

SCHLICHTING, H. 1968 *Boundary-Layer Theory*, 6th edn. McGraw-Hill.

SHEPPARD, P. A. 1956 Airflow over mountains. *Q. J. R. Met. Soc.* **82**, 528–529.

SNYDER, W. H., BRITTER, R. E. & HUNT, J. C. R. 1980 A fluid modelling study of the flow structure and plume impingement on a three-dimensional hill in stably stratified flow. In *Proc. 5th Intl Conf. on Wind Engng, Fort Collins* (ed. J. E. Cermak), vol. 1, pp. 319-329. Pergamon.

SNYDER, W. H., THOMPSON, R. S., ESKRIDGE, R. E., LAWSON, R. E., CASTRO, I. P., LEE, J. T., HUNT, J. C. R. & OGAWA, Y. 1985 The structure of strongly stratified flow over hills: dividing-streamline concept. *J. Fluid Mech.* **152**, 249–288.

SU, C. H. 1975 Some dissipative effects on stratified shear flows over an obstacle. *Phys. Fluids* **18**, 1081–1084.

SYKES, R. I. 1978 Stratification effects in boundary layer flow over hills. *Proc. R. Soc. Lond.* A **361**, 225–243.

TANEDA, S. 1956 Experimental investigation of the wake behind a sphere at low Reynolds numbers. *J. Phys. Soc. Japan* **11**, 1104–1108.

THAMES, F. C., THOMPSON, J. F., MASTIN, C. W. & WALKER, R. L. 1977 Numerical solutions for viscous and potential flow about arbitrary two-dimensional bodies using body-fitted coordinate systems. *J. Comput. Phys.* **24**, 245–273.

YIH, C.-S. 1960 Exact solutions for steady two-dimensional flow of a stratified fluid. *J. Fluid Mech.* **9**, 161–174.

YIH, C.-S. 1980 *Stratified Flows*. Academic.